Journal of the European Ceramic Society 38 (2018) 201–210

Contents lists available at ScienceDirect

Journal of the European Ceramic Society

journal homepage: www.elsevier.com/locate/jeurceramsoc

Microstructure and elastic modulus of electrospun Al_2O_3-SiO_2-B_2O_3 composite nanofibers with mullite-type structure prepared at elevated temperatures

Xiaolei Song, Wensheng Liu*, Shuheng Xu, Juan Wang, Bing Liu, Qingshan Cai, Siwei Tang, Yunzhu Ma*

State Key Laboratory of Powder Metallurgy, Central South University, Changsha 410083, China

ARTICLE INFO

Keywords:
Fibers
Electrospinning
Microstructure
Flexibility
Mullite-type structure

ABSTRACT

In the present work, Al_2O_3-SiO_2-B_2O_3 composite nanofibers with mullite-type structure were prepared using electrospinning technique. The microstructure and elastic modulus of the composite nanofibers obtained at elevated temperatures were studied. The results showed that $Al_4B_2O_9$ phase formed at 900 °C and then transformed to $Al_{18}B_4O_{33}$ at 1100 °C. Mullite was also detected in the nanofibers prepared at 1100 °C. Amorphous SiO_2 existed in all samples even the calcination temperature reached up to 1400 °C. The continuous and uniform structure of the composite nanofibers was kept after calcining at different temperatures, while rougher surface was evident due to the growth of the grain caused by the elevated temperature. An increase of elastic modulus of the samples from 9.47 ± 1.91 GPa to 27.30 ± 2.61 GPa was observed when calcination temperatures increased from 800 °C to 1400 °C.

1. Introduction

Continuous mullite ($3Al_2O_3{\cdot}2SiO_2$) fibers, as a kind of promising ceramic materials, have been used in various areas, including insulation, filtration, catalyst and reinforcement of metals, ceramics and resins due to their outstanding dielectric properties, chemical stability, low thermal conductivity and excellent high temperature properties [1–3]. Amongst all the physical properties of ceramic fibers, good flexibility is essential to allow the fiber products to be converted into required shapes and forms, and expands their applications eventually [1,4]. With respect to mullite fibers, a serious problem is their relatively high elastic modulus [4], which lead up to a low flexibility and restrict their applications consequently.

To date, researches prove that diminishing the grain sizes is an available approach to improve the flexibility of mullite fibers [1,5]. To achieve this purpose, adding B_2O_3 into the mullite was investigated. EA Richards et al. [5] found that B_2O_3 is the most effective additive to decrease the grain sizes of mullite fibers compared with P_2O_5, Cr_2O_3 and their mixture. They also confirmed that small grain size was correlated with high tensile strength of the fibers. Though the addition of B_2O_3 significantly decreased the mullite formation temperature, the boron doped mullite fibers still showed enormous advantages when they were converted into textiles (i.e. yarn, sleevings or fabrics) owing to their relatively high flexibility. Currently, the most widely known flexible commercial ceramic fibers in Al_2O_3-SiO_2-B_2O_3 ternary system are Nextel™ 312 fibers produced by 3 M Company (USA) [4,6]. The chemical composition of the fibers in wt.% is 62% Al_2O_3, 24% SiO_2 and 14% B_2O_3. The filament tensile modulus of Nextel™ 312 fibers is about 150 GPa, which is the smallest among the Nextel™ ceramic oxide fibers, indicating the best flexibility and lowest weaving difficulty. Nextel™ 440 fiber is another type of Al_2O_3-SiO_2-B_2O_3 composite fiber with lower B_2O_3 content (2 wt.%) and a higher modulus (190 GPa) [4]. With the exception of the good flexibility, the introduction of B_2O_3 also decreases the density of mullite fibers. This feature is benefit to reduce the total weight of those objects which the Al_2O_3-SiO_2-B_2O_3 ternary ceramic fibers are used in large amount.

For ceramic fibers, which involve mullite fibers undoubtedly, reducing their diameters was also a meaningful method to improve their flexibility [1,7]. Particularly, ceramic nanofibers, apart from the good flexibility, are also gifted with larger surface area to volume, lower density, lower conductivity of heat and other superior properties, and have drawn a lot of attention [8,9]. Obviously, the smaller diameters of ceramic fibers are related to the disparate preparation technology. The conventional techniques used to prepare ceramic fibers are melt extraction [10], melt spinning [11,12], pyrolysis of cured polymer fiber [13] and sol-gel processing [14–16], etc. However, such methods are

* Corresponding authors.
E-mail addresses: liuwensheng@csu.edu.cn (W. Liu), yunzhum@163.com, zhuzipm@csu.edu.cn (Y. Ma).

http://dx.doi.org/10.1016/j.jeurceramsoc.2017.08.007
Received 28 June 2017; Received in revised form 29 July 2017; Accepted 3 August 2017
Available online 04 August 2017

still not available to produce ceramic fibers in nano-scale independently as investigated previously. Consequently, the method of a combination of electrospinning and sol-gel processing was developed in the past two decades to prepare continuous ceramic nanofibers. Dai et al. [17] prepared ultra-fine alumina-borate oxide fibers for the first time using this method. Soon afterwards, other ceramic nanofibers such as SiO_2 [18], Al_2O_3 [19], ZrO_2 [20] and so on were derived. As to electrospinning technique, it involves the use of a high voltage to charge the surface of a polymer solution droplet through a spinneret, and then a liquid jet ejects. The jet is stretched to form continuous and ultrafine fibers due to the electric field force acting on them. While fabricating ultrafine ceramic fibers using this method, precursor sol is initially added into a polymer additive solution to acquire the composite spinning solution. Then the spinning solution is electrospun to obtain the as-spun composite nanofibers and the as-spun fibers are calcined to produce the desired products. To summarize, this method has been demonstrated to be an effective way to generate various kinds of ceramic nanofibers with high purity, good homogeneity, fine grain sizes and sufficiently small diameters, and has been regarded as a promising technique in generating continuous ultrafine ceramic fibers in the future.

As has been introduced, mullite nanofibers were also prepared by electrospinning combined with sol-gel method. Wu et al. [21] prepared high purity polycrystalline mullite nanofibers with diameters of about 200 nm using aluminum nitrate (AN), aluminum isoproxide (AIP) and tetraethyl orthosilicate (TEOS) as raw materials. They focused on the influence of the PVP content on the morphology development of mullite nanofibers and they observed that large grains formed in the fibers after heat treatment at 1200 °C. M. Mohammad Ali Zadeh et al. [22,23] also studied the impact of the proportions of polymer additives on the properties of spinning solution and morphology of mullite precursor nanofibers, but their fiber products were not uniform and could not retain a stable structure under high temperature. Chen et al. [24] fabricated mullite fibers with diameters ranging from 400 nm to 10 um using electrospinning technique. They considered that the most convenient way to obtain fibers with well-controlled diameters was to control the solid concentration and the rheology of the mullite sol. Peng et al. [25] prepared uniaxially aligned mullite fibers by electrospinning, but the average diameter of the fibers calcined at 1300 °C was 1.78 um, which were not in nanoscale apparently. Based on these introductions it can be seen that researchers are still focusing on fabricating pure mullite without the additions of second phases, which means that continuous mullite nanofibers with B_2O_3 added synthesized by electrospinning have not raised much interest yet. S. Tanriverdi et al. [26] once prepared electrospun ceramic nanofibers in Al_2O_3-SiO_2-B_2O_3 ternary system with a Al_2O_3:SiO_2:B_2O_3 ratio of 1:8:1. But the fibers could hardly be regarded as a type of mullite fibers since SiO_2 had crystallized at 1000 °C due to its large amount and the final products lost fiber-like structure after calcined at temperatures beyond 1000 °C. Apart from that, the synthesis of Al_2O_3-SiO_2-B_2O_3 composite nanofibers has never been reported. Thus, it is meaningful to prepare the Al_2O_3-SiO_2-B_2O_3 composite nanofibers with mullite-type structure. Additionally, little attention has been paid on the mechanical properties of the electrospun mullite nanofibers and little research has been done regarding the relationship between elastic modulus and calcination temperatures. Consequently, the aim of the present work was to prepare mullite-type nanofibers in Al_2O_3-SiO_2-B_2O_3 ternary system with good flexibility. The phase transformation, microstructure evolution and room temperature elastic modulus of the composite nanofibers after calcining at elevated temperature were investigated.

2. Experimental

2.1. Synthesis of stable spinning solution

Aluminum acetate ($Al(OH)_2(OOCCH_3)\cdot 1/3H_3BO_3$) purchased from Strem Chemicals, Inc. (Boston,USA) was used as the sources of alumina and boron oxide. Boric acid contained in the aluminum acetate acts as a stabilizer. Tetraethyl orthosilicate (TEOS) with a SiO_2 content of 28 wt. % offered by Xilong Chemical Co., Ltd. (Guangzhou, China) was used as the silica source. Deionized water and pure ethanol were used as the solvent to prepare the composite precursor sols. The molar ratio of Al:Si:B of the target nanofibers was designed to be 3:1:1. To obtain homogeneous precursor sols, aluminum acetate stabilized with boric acid, TEOS, deionized water and pure ethanol were mixed together simultaneously. The mass percentages of the four materials in the mixture were 15, 7.2, 38.9 and 38.9 wt.%, respectively. The mixture solution was stirred at 40 °C for 12 h to obtain the composite precursor sol. Polyvinyl pyrrolidone (PVP, Mw = 1,300,000) provided by Bodi Chemical Reagent Plant (Tianjin, China) was applied as the polymer additive. It was added into alcohol and stirred at room temperature for 3 h to acquire a 16 wt.% PVP alcohol solution. Then the PVP solution was mixed with the precursor sol with a mass ratio of 3:2 and stirred for 1 h to obtain a composite spinning solution which was homogeneous and suitable for electrospinning.

2.2. Electrospinning and calcination

The composite spinning solution was transferred into a plastic syringe equipped with a metallic needle. The needle was connected to a negative voltage supply. During electrospinning, the voltage supply was set to generate a voltage of −7.45 kV and the feeding rate controlled by a syringe pump was kept at 0.45 ml/h. A piece of aluminum foil was used as the collector and the distance between the needle tip and the collector was 15 cm. After electrospinning, the as-spun composite nanofibers mats were dried by an oven at 50 °C for 5 h to remove the residual solvent. The dried fiber mats were put in Al_2O_3 plates and calcined in a muffle furnace from room temperature to 800 °C in air circumstance with a heating rate of 5 °C/min. After calcining at 800 °C for 1 h, PVP and organic matters existed in the as-spun fibers were basically decomposed and removed. Then the nanofibers were calcined at temperatures varied from 800 to 1400 °C for an extra 1 h to obtain the Al_2O_3-SiO_2-B_2O_3 composite nanofibers.

2.3. Characterization

The X-ray powder diffraction (XRD) data of calcined samples were recorded by a diffractometer (D8 Advance, Bruker, German) with CuKα radiation in the region of $10 < 2\theta < 80^{\circ}$. Diffraction peaks were indexed with Jade 6.0 software. Fourier transform infrared (FT-IR) absorption spectra of the calcined nanofibers were recorded using a spectrometer (Model 6700, Nicolet, USA) at wave number ranged from 400 to 1500 cm^{-1}. The calcined fibers were ground to powders to prepare KBr pelltes for FT-IR measurements. The morphology of the nanofibers was examined by scanning electron microscopy (SEM) (Quanta FEG 250, FEI, USA) and transmission electron microscopy (TEM) (JEM-2100F, JEOL, Japan). To prepare SEM samples, the as-spun nanofibers should not be exposed to air for too long to avoid the absorption of the moisture and protect the fiber morphology. The calcined nanofibers were sputtered with relatively thicker gold layer due to the low conductivity. The diameters of the nanofibers were calculated using the image analysis software Image J. As to the samples to be detected by TEM, calcined fibers were placed into ethanol and treated by ultrasonic subsequently. The suspensions with separated nanofibers were obtained and then were dripped on carbon-coated copper grids, where the nanofibers were left for TEM examination. The elastic modulus of a single ceramic nanofiber was measured using the three-point bending method by atomic force microscope (AFM) (Multimode 8, Veeco, USA) under the force mode. For AFM samples preparation, Al_2O_3-SiO_2-B_2O_3 nanofibers were placed into ethanol and ultrasonic treated for 30 min to obtain a suspension. The suspension was dropped on a customized silicon wafer with many etched grooves, each of which

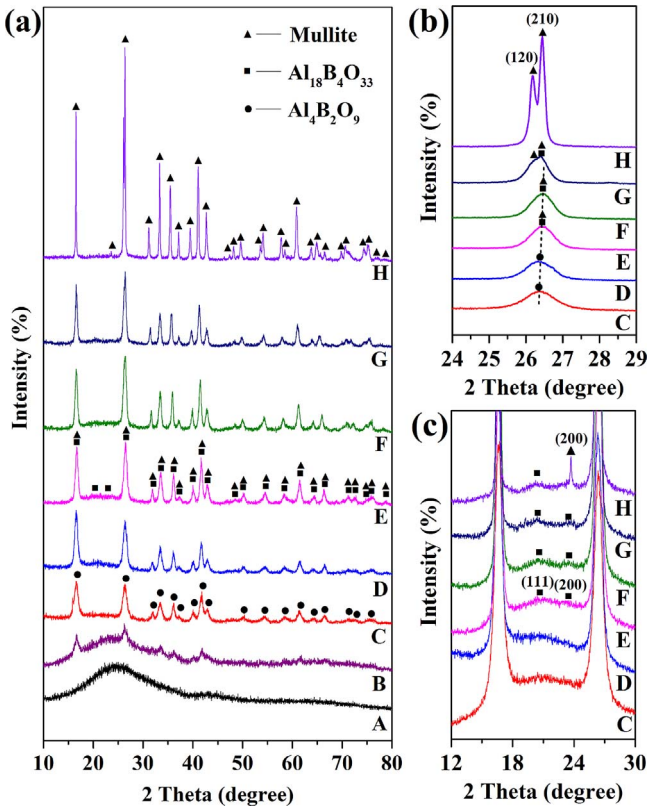

Fig. 1. XRD patterns of Al_2O_3-SiO_2-B_2O_3 nanofibers calcined at elevated temperatures: (a) patterns in the region of $10 < 2\theta < 80^\circ$; (b) patterns at around the 2θ of 26°, showing the evolution of the nearby diffraction peaks; (c) patterns in the region of $12 < 2\theta < 30^\circ$, exhibiting the presence of amorphous SiO_2 and $Al_{18}B_4O_{33}$ phase. Patterns A to H were obtained after calcining the fibers at 800, 825, 900, 1000, 1100, 1200, 1300 and 1400 °C, respectively.

was 4 μm wide. Then the silicon wafer was dried by a heating lamp. The nanofibers deposited right across the grooves were selected to be tested. The spring constant and deflection sensitivity of the cantilever we used were obtained from the force curve of a sapphire standard sample offered by Veeco Co. They were measured to be 155.11 N/m and 35.622 nN/V, respectively. Five readings were taken from each fiber to obtain the modulus value.

3. Results and discussion

3.1. Crystal phase and chemical structure

Fig. 1 shows the XRD patterns of the Al_2O_3-SiO_2-B_2O_3 nanofibers calcined between 800 °C and 1400 °C. As observed from Fig. 1(a), there was no distinct diffraction peak appearing on pattern of the sample calcined at 800 °C(A in Fig. 1(a)), the broad hump revealed between the 2θ of about 12° and 38° suggesting the presence of amorphous phase. This amorphous phase was identified as amorphous silica. When the calcination temperature increased to 825 °C (B in Fig. 1(a)), some weak diffraction peaks emerged, which indicated the formation of crystalline phases, but it was difficult to find out their identities. After calcined at 900 °C (C in Fig. 1(a)), the weak diffraction peaks emerged at 825 °C turned to be obvious. The diffraction peaks were detected as $Al_4B_2O_9$ (card #47-0319) phase. Sowman and his co-workers [27] once reported that B_2O_3 reacted with Al_2O_3 to form aluminum borate $9Al_2O_3{\cdot}2B_2O_3$ ($Al_{18}B_4O_{33}$) first when it was added to mullite gels to prepared ceramic fibers. However, researches about alumina borate materials showed that $Al_4B_2O_9$ phase generated first commonly and only when reaction temperature was higher than the melting point of $Al_4B_2O_9$ (about 1030 °C), can $Al_4B_2O_9$ phase slowly convert to $Al_{18}B_4O_{33}$ phase [28,29]. What's more, some researches regarding the structure evolution about the Al_2O_3-SiO_2-B_2O_3 ternary system also showed that $Al_4B_2O_9$ phase generated first and then transformed to $Al_{18}B_4O_{33}$ phase gradually [30,31]. Our results are consistent with these conclusions.

At 1000 °C (D in Fig. 1(a)), the crystallinity of $Al_4B_2O_9$ phase increased, which indicated that the structure was stable. As reported, mullite derived from monophasic gel usually formed at about 980 °C [32], but it could not be detected from the XRD pattern. For most crystal planes in $Al_4B_2O_9$ and pure mullite (card #15-0076), the d-spacings are nearly equal, which makes them difficult to be distinguished. However, for those crystal planes with larger d-spacing differences, the corresponding split peaks could not be observed neither in Al_2O_3-SiO_2-B_2O_3 ternary system investigated by Zhang et al. [31]. They ascribed this to that the boron-doped mullite was a solid solution which includes some units with the same structure as mullite and $Al_4B_2O_9$, instead of a simple mixture of pure mullite and $Al_4B_2O_9$. Even so, it was still unable to confirm the formation of the mullite phase in our nanofibers after calcining at 1000 °C by XRD measurement.

When calcination temperature reached to 1100 °C (E in Fig. 1(a)), the pattern exhibited similar features as that of 1000 °C, but four weak diffraction peaks emerged at the 2θ of about 20.3, 23.7, 48.5 and 75.1°, which indicated that $Al_{18}B_4O_{33}$ phase (card #32-0003) formed at this temperature. This was consistent with the above conclusion about the phase transition from $Al_4B_2O_9$ to $Al_{18}B_4O_{33}$. In addition, the relative intensities of the diffraction peaks at the 2θ of about 16° and 26° reversed as well. To our knowledge, the intensity of the first peak is stronger than that of the second one for $Al_{18}B_4O_{33}$, but a reversal of the ratio of intensities of the two peaks can be observed for mullite. Sowman [27] discussed the relative intensities of the two diffraction peaks from XRD patterns of Al_2O_3-SiO_2-B_2O_3 fibers lie between mullite and aluminum borate, and pointed out that the ratio of relative intensities of the two diffraction peaks moved toward that of mullite as temperature increased. It is clear that Al_2O_3 will react with SiO_2 to form mullite with the increasing temperature. That is to say, the formation of mullite could be confirmed by observing the relative intensities of the diffraction peaks at the 2θ of about 16° and 26° in Al_2O_3-SiO_2-B_2O_3 ternary system. Beyond that, no other diffraction lines could be used to identify the mullite phase. This was because that the diffraction lines of mullite are partially similar to or even overlapped with that of $Al_{18}B_4O_{33}$ due to their similar crystal structure and lattice parameters [31]. To summarize, it could be concluded that mullite phase had formed at 1100 °C.

After calcined at 1200 and 1300 °C (F and G in Fig. 1(a)), the intensities of the second diffraction peaks were much stronger than the first ones, which indicated that the increasing crystallinity and content of mullite phase. However, all other diffraction peaks in the patterns were much closer to $Al_{18}B_4O_{33}$. Although $Al_{18}B_4O_{33}$ decomposed constantly with calcination time extended, it was still the dominant phase after calcining 1 h at 1200 and 1300 °C. While at temperature up to 1400 °C (H in Fig. 1(a)), nearly pure mullite (card #15-0076) was obtained (the impurity phase were discussed below), which meant that a large proportion of B_2O_3 in the calcined composite nanofibers evaporated.

The patterns of nanofibers obtained at different temperatures at around the 2θ of 26° are exhibited in Fig. 1(b), which verified that the phase evolution discussed above was reliable. The peak position shifted to higher diffraction angle when temperature increased from 900 °C to 1100 °C, which also confirmed that $Al_4B_2O_9$ transformed to $Al_{18}B_4O_{33}$. When temperature increased to 1300 °C, the peaks shifted back to lower angles, revealing that mullite was the main component. Specially, the diffraction peak in sample of 1300 °C was asymmetrical (G in Fig. 1(b)). The asymmetrical feature was ascribed to the two faintly split peaks emerged at the 2θ of 26.19 and 26.38° corresponding to the crystal planes (120) and (210) of mullite. At 1400 °C, the peaks correlated to the (120) and (210) crystal planes were split and became sharpening, which indicated the increase of crystallinity of mullite.

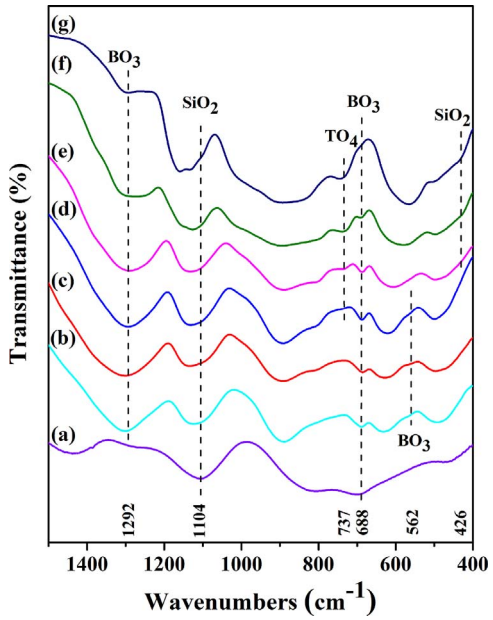

Fig. 2. FT-IR spectra of the Al_2O_3-SiO_2-B_2O_3 nanofibers calcined at different temperatures: (a) 800 °C; (b) 900 °C; (c) 1000 °C; (d) 1100 °C; (e) 1200 °C; (f) 1300 °C; (g) 1400 °C.

The enlarged view of the patterns in the region of $12 < 2\theta < 30°$ is showed in Fig. 1(c). It could be seen that humps stood for amorphous SiO_2 existed after calcining from 900 to 1400 °C, despite the formation and transformation of crystal phases. Besides, for the pattern obtained at1400 °C (H in Fig. 1(c)), the peak at the 2θ of 20.3° did not vanish, which revealed that $Al_{18}B_4O_{33}$ did not decompose completely. The initial mol ratio of Al:Si for the Al_2O_3-SiO_2-B_2O_3 nanofibers was designed as 3:1, which was identical to that of mullite. Therefore, amorphous SiO_2 would always be as long as alumina borate phase did not vanish theoretically. In fact, such phase composition was benefit for Al_2O_3-SiO_2-B_2O_3 nanofibers to keep a stable structure at high temperatures because the presence of amorphous SiO_2 could prevent the growth of crystal grains and promote the closure of tiny holes and cracks effectively.

FT-IR spectra of the Al_2O_3-SiO_2-B_2O_3 nanofibers obtained at different temperatures in the range of 1500–400 cm^{-1} were measured to study the chemical structure evolution. Fig. 2 displays the spectra and Table 1 lists the corresponding band locations and assignments. At 800 °C, the band appeared at 1433 cm^{-1} was corresponded to the antisymmetric stretching vibrations of BO_3 groups and the band at 698 cm^{-1} was due to the symmetric bending vibrations of BO_3 groups [30,33–35]. After calcining at 900 °C, absorption bands at 890, 630 and 493 cm^{-1} ascribed to the Al—O stretch in AlO_4, O—Al—O bend in AlO_4 and Al—O—Al bend in AlO_6 emerged [36–38]. The above mentioned structural units including BO_3, AlO_4 and AlO_6 are the main components of $Al_4B_2O_9$ phase [33], suggested that $Al_4B_2O_9$ formed at this temperature. For spectra from 900 to 1200 °C, no reliable feature showed the transition from $Al_4B_2O_9$ to $Al_{18}B_4O_{33}$, but the sharpening of bands located at around 688 cm^{-1} with the increasing calcination temperatures indicated that the nanofibers were becoming more crystalline on alumina borate phase. Additionally, absorption bands at around 562 cm^{-1} ascribed to the B—O bending vibrations in BO_3 units [30,35] in samples of 900–1100 °C vanished in the sample obtained at 1200 °C indicated that alumina borate was decomposing when calcination temperatures increased. However, upon further heating to 1400 °C, though the bands at 1294 and 687 cm^{-1} became shoulders due to the decomposition of $Al_{18}B_4O_{33}$, $Al_{18}B_4O_{33}$ still existed. As deduced in XRD analyses, for the products involved in the current study, if $Al_{18}B_4O_{33}$ do not decompose completely, amorphous SiO_2 will not vanish either. It was verified by FT-IR accurately since the absorption bands at around 1104 cm^{-1}, which were assigned to the stretching vibration of Si—O—Si in amorphous SiO_2 [36,38], were found in all samples though their intensities weakened with the increasing calcination temperature. Besides, when temperature exceeded 1200 °C, shoulder peaks appeared at around 426 cm^{-1} was ascribed to the bending vibration of Si—O—Si in SiO_2 as well [38]. These results revealed that the amount of amorphous SiO_2 decreased gradually but did always exist after calcining at elevated temperatures as XRD showed. When the nanofibers were calcined at 1100 °C, the absorption bands around 1007 cm^{-1} and 737 cm^{-1} corresponded to the stretching vibration of Si-O in SiO_4 and bending vibration of T-O-T in TO_4 emerged [37,38]. The TO_4 units, known to act as the nucleation sites for mullite, demonstrated that mullite had already formed at 1100 °C. And when calcination temperature increased, the peaks at around 737 cm^{-1} broadened, which exhibited that the amount and crystallinity of mullite increased simultaneously.

3.2. Morphology and microstructure

SEM images of as-spun composite nanofibers and Al_2O_3-SiO_2-B_2O_3 nanofibers heated at set temperatures are shown in Fig. 3. It could be observed from Fig. 3(a) that continuous fibers with smooth surface and cylindrical morphology were successfully prepared. The fibers were randomly distributed with diameters in the range of 700–1050 nm and an average diameter of about 865 nm. The well-proportioned diameter distribution and uniform structure were attributed to the high chemical homogeneity and suitable rheological property of the composite spinning solution, as well as the good electrospinning parameters and conditions [39]. As observed in Fig. 3(b), the nanofibers retained

Table 1
Band locations and assignments derived from FT-IR spectra of the nanofibers calcined at different temperatures.

800 °C	900 °C	1000 °C	1100 °C	1200 °C	1300 °C	1400 °C	Assignment [30,33–38]
1433	1302	1299	1293	1291	1292	1294	B—O stretch (BO_3) [30,33,34]
–	–	–	–	1148	1153	1161	Si—O stretch (SiO_4) [37]
–	1134	1136	1136	1131	1131	1133	Si—O stretch (SiO_4) [37]
1104	1106	1104	1104	1110	1109	1107	Si—O stretch (SiO_2) [36,38]
–	–	–	1004	1009	1011	1011	Si—O stretch (SiO_4) [37,38]
–	890	892	894	892	892	894	Al—O stretch (AlO_4) [37,38]
804	810	801	804	801	799	820	Al—O stretch (AlO_4) [37,38]
–	–	–	737	737	737	738	T—O—T bend (TO_4) [37,38]
698	689	685	689	688	688	687	B—O bend (BO_3) [30,35]
–	630	625	622	616	616	608	O—Al—O bend (AlO_4) [37,38]
–	–	–	–	594	564	563	Al—O stretch (AlO_6) [37,38]
–	562	558	561	–	–	–	B—O bend (BO_3) [30,35]
–	493	493	499	496	496	499	Al—O—Al bend (AlO_6) and
466	463	466	468	466	468	466	O—Si—O bend (SiO_4) [37,38]
–	–	–	–	426	429	435	Si—O—Si bend (SiO_2) [38]

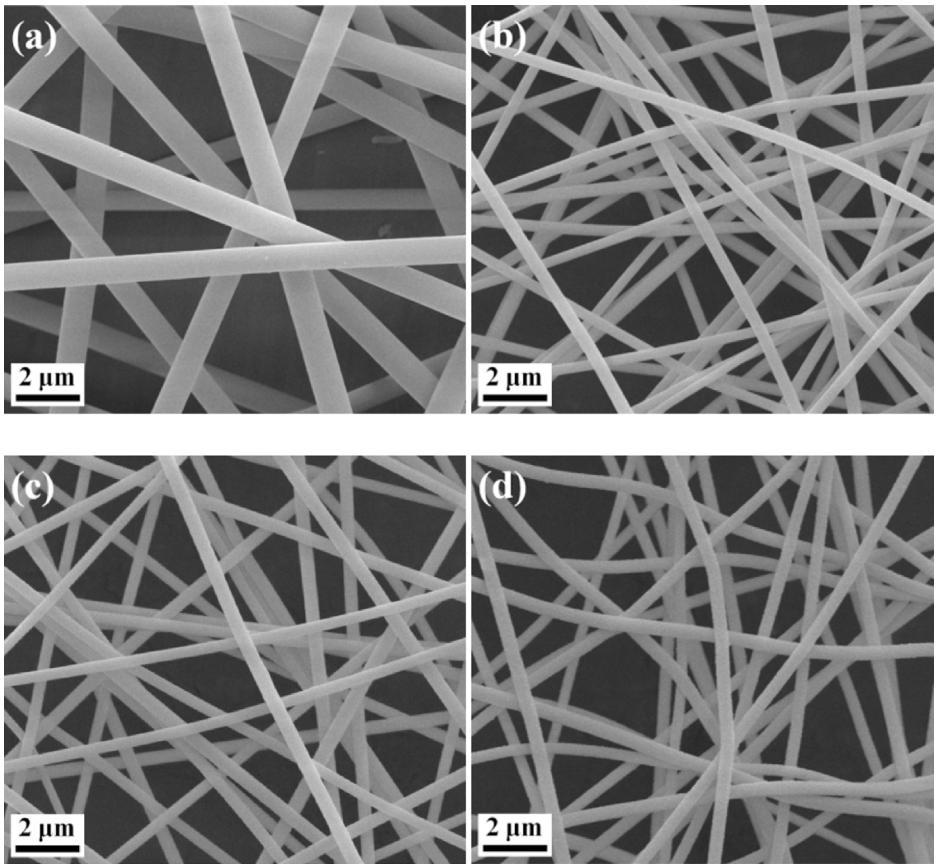

Fig. 3. SEM images of (a) as-spun composite nanofibers and Al_2O_3-SiO_2-B_2O_3 nanofibers calcined at (b) 1000 °C, (c) 1200 °C and (d) 1400 °C.

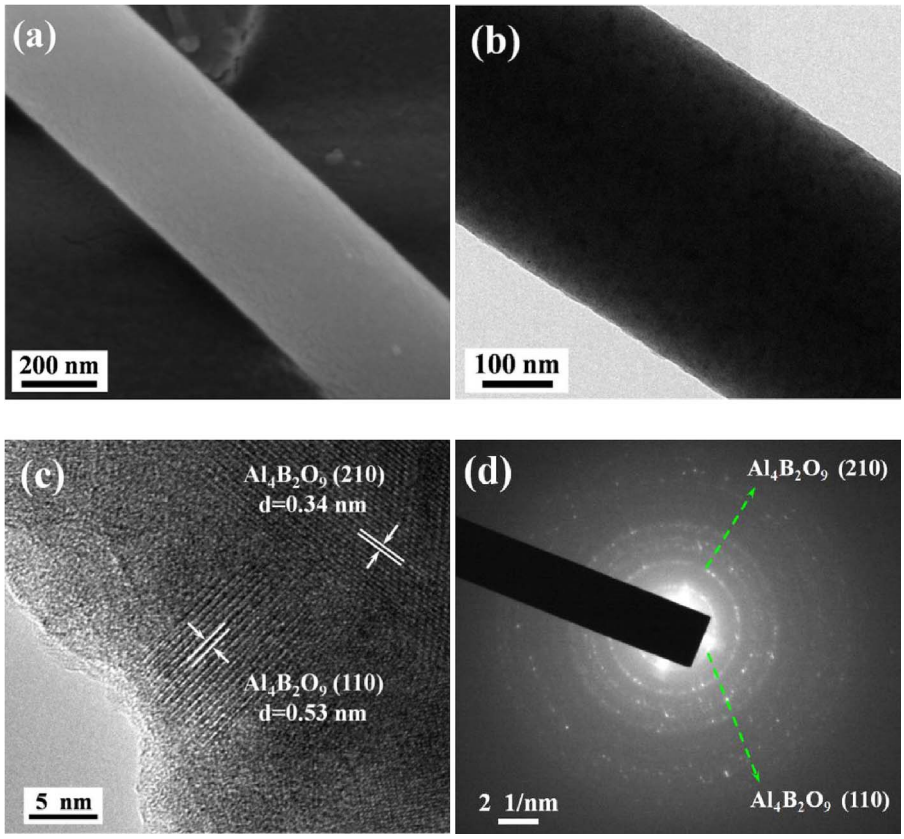

Fig. 4. (a) SEM of surface morphology, (b) TEM, (c) HRTEM and (d) ED pattern of the Al_2O_3-SiO_2-B_2O_3 nanofibers calcined at 1000 °C.

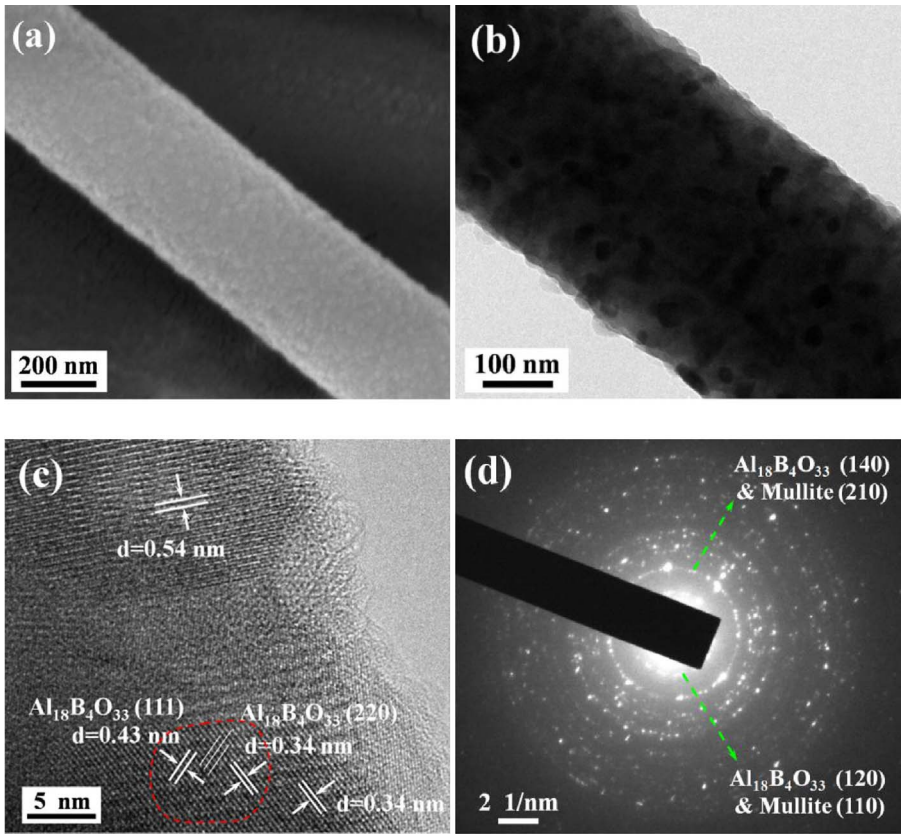

Fig. 5. (a) SEM of surface morphology, (b) TEM, (c) HRTEM and (d) ED pattern of the Al_2O_3-SiO_2-B_2O_3 nanofibers calcined at 1200 °C.

continuous and cylindrical morphology after calcining at 1000 °C, despite a sharp decrease in diameter compared to the as-spun fibers. The decreased diameters were caused by the decomposition of PVP and organic groups during calcination, which confirmed that PVP was a good structure-directing polymer additive. While for the sample calcined at 1200 °C and 1400 °C, the structure of the nanofibers remained stable as observed in Fig. 4(c) and (d). This was superior to the electrospun pure mullite nanofibers prepared by Iranian scientists since their fibers had become discontinuous and irregular at 1400 °C [23]. One reason for such phenomenon was that mullite formed at 1000 °C in their study, which resulted in larger grain sizes. Another reason should be that the relatively larger diameters of our nanofibers kept the better structural stability. Notably, the stable structure is beneficial to the application of the Al_2O_3-SiO_2-B_2O_3 nanofibers.

To explore the microscopic differences between the Al_2O_3-SiO_2-B_2O_3 nanofibers prepared at 1000, 1200 and 1400 °C, the SEM of surface morphology, TEM, HR-TEM and electronic diffraction (ED) pattern images are displayed in Figs. 4–6, respectively.

For the sample calcined at 1000 °C, both Fig. 4(a) and (b) allowed us to confirm that the nanofibers were uniform with smooth surface, which were beneficial to keeping their mechanical properties. As we know, when as-spun composite nanofibers are calcining, many physical and chemical reactions take place, including the removal of residual water and the decomposition of boric acid, acetate radical, PVP and other organic groups that existed. Some of these reactions were drastic, so the rapid release and diffusion of gaseous products may cause some non-repaired defects to the nanofibers. In terms of our fibers, when heated up to 800 °C with a heating rate of 5 °C/min, the gaseous products tended to diffuse easily. Thus, the surface was uniform and smooth. And the good feature remained after the calcination of 1000 °C for 1 h because the crystal grains were small. As observed in Fig. 4(b), the sizes of $Al_4B_2O_9$ grains ranged from 4 to 25 nm. The grains were disconnected with each other because they were surrounded by amorphous silica normally. HRTEM image shown in Fig. 4(c) revealed that the crystallographic orientations of $Al_4B_2O_9$ phase were mainly in (110) and (210) crystal planes. And ED pattern verified that $Al_4B_2O_9$ was the main phase (Fig. 4(d)), which was in consistent with the XRD result.

As obviously shown in Fig. 5(a), a lot of tiny particles appeared on the surface of the nanofibers calcined at 1200 °C. According to the XRD and FT-IR results, $Al_4B_2O_9$ transformed to $Al_{18}B_4O_{33}$ and mullite when temperature was 1100 °C and the crystallinity increased when calcination temperature reached to 1200 °C. All these results implied that the grains of the crystal phase became larger. This was why the fiber surface became rough. This inference could also be illustrated by comparing the TEM images of fibers obtained at the two temperatures. In Fig. 5(b), grains distributed in a disordered manner had sizes varied from 10 to 65 nm and an average size of approximately 35 nm, which were much smaller than that of the grains in pure mullite nanofibers (~100 nm) displayed in Wu's study [21]. The existence of amorphous SiO_2 was confirmed by the HRTEM image of the fiber (Fig. 5(c)). What is more, the verdict that diffraction lines of $Al_{18}B_4O_{33}$ and mullite are difficult to be distinguished mentioned in XRD analyses could be testified in Fig. 5(c) likewise. For example, the grain at the top of Fig. 5(c) showed a 0.54 nm d-spacing of the crystal plane, which was equal to that of (110) crystal plane for $Al_{18}B_4O_{33}$, as well as that of (120) crystal plane for mullite. Therefore, to identify the two crystal phases by this crystal plane was impossible. As we know, with the exception of the relative intensities of two diffraction peaks, another significant difference between the two crystal phases is that a (111) crystal plane with d-spacing of 0.43 nm presents in $Al_{18}B_4O_{33}$ particularly. At the bottom of Fig. 5(c), the (111) crystal plane was detected, but it could not be used to testify that the entire grain belonged to $Al_{18}B_4O_{33}$. This was because that aluminum borate was regarded as an epitaxial substrate for the nucleation and growth of mullite due to their similar crystal structure and lattice parameters as studied before [27,40]. The ED pattern displayed in Fig. 5(d) showed that the diffraction rings corresponding to the (111), (200) and (031) crystal planes for $Al_{18}B_4O_{33}$ could not be observed, which made the pattern seemed much similar to that of

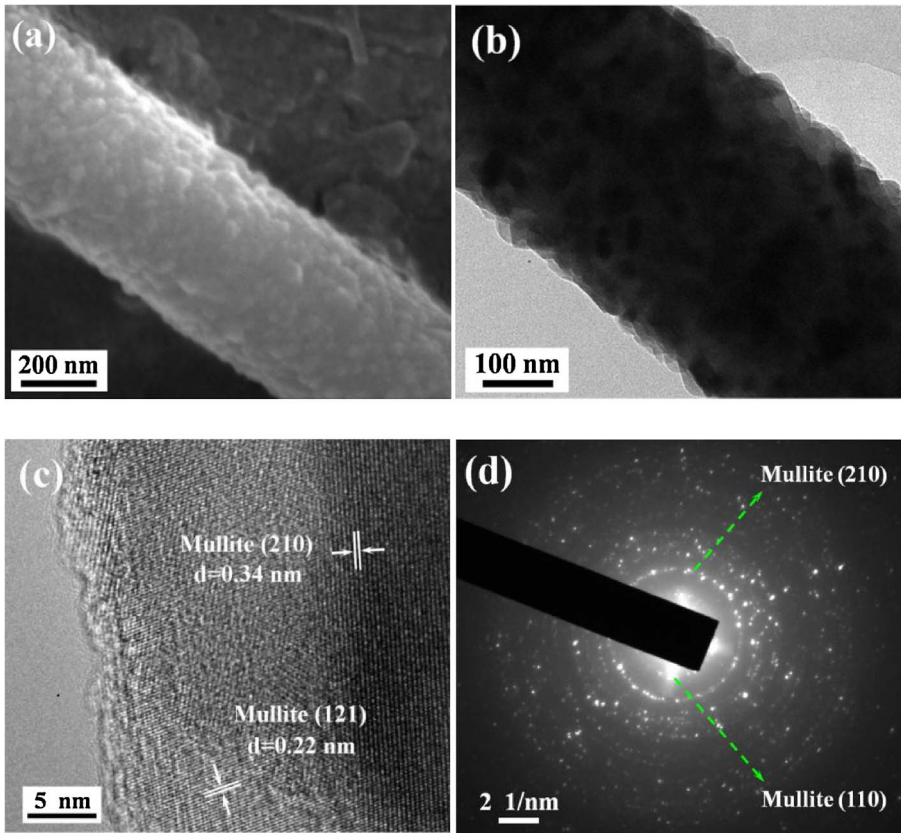

Fig. 6. (a) SEM of surface morphology, (b) TEM, (c) HRTEM and (d) ED pattern of the Al_2O_3-SiO_2-B_2O_3 nanofibers calcined at 1400 °C.

mullite phase. One reason for this was that the three diffraction rings were slight inherently (not shown in this work). Another reason might be that the amount of pure $Al_{18}B_4O_{33}$ phase, rather than mullite-type $Al_{18}B_4O_{33}$ phase, was too small to generate these diffraction rings.

For the nanofibers prepared at 1400 °C, the particles on the surface were larger and more irregular as shown in Fig. 6(a). In Fig. 6(b), the grains with sizes in the range of 30–100 nm were connected to each other mostly. Furthermore, many elongated grains generated due to the anisotropic grain growth in Al_2O_3-SiO_2-B_2O_3 ternary system [40]. Obviously, the growth of crystal grains led to the rough surface feature. Since mullite had became the dominant phase at this temperature, the grains in the HRTEM image (Fig. 6(c)) were identified to be mullite grains and they grew up mainly in the direction of (210) and (121) crystal faces. The ED patterns (Fig. 6(d)) further confirmed what have been observed.

3.3. Elastic modulus and flexibility

Fig. 7(a) shows the 3D AFM image of a single Al_2O_3-SiO_2-B_2O_3 nanofiber suspended over a groove on silicon wafer. It was evident that the fiber attached closely to the surface of the silicon wafer and deposited right across the groove, which demonstrated that the beam structure was desired. As far as we know, this method of acquiring the elastic modulus of electrospun nanofibers have been studied by many researchers [41–43], who normally focused on the relationship between modulus values and fiber diameters and concluded that elastic modulus increased when fiber diameter reduced to a certain value. Therefore, in order to avoid the effects of fiber diameters on modulus of the different samples, nanofibers with similar diameters were selected to be measured. In addition, an intact force curve obtained by AFM is composed of an approaching part and a retracting part as exhibited in Fig. 7(b), of

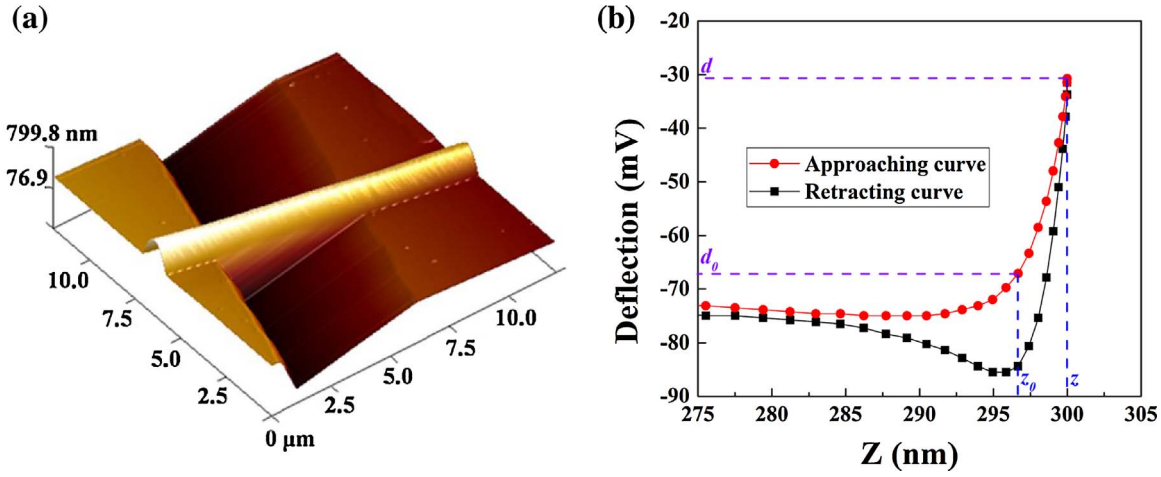

Fig. 7. (a) 3D AFM image of a single Al_2O_3-SiO_2-B_2O_3 nanofiber suspended over a groove of silicon wafer and (b) a representative force curve of a single nanofiber obtained by AFM.

which the approaching part is appropriate be used for calculating the elastic modulus. The modulus value was calculated using the following formula:

$$E = \frac{FL^3}{192\delta I} \quad (1)$$

where F is the force applied, L is the suspended length, δ is the deflection of the beam at midspan, and I is the second moment of area of the beam. The applied force F was calculated by:

$$F = k(d - d_0)m \quad (2)$$

where k is the spring constant of the cantilever, $d - d_0$ is the deflection voltage and m is the deflection sensitivity, respectively. δ was calculated by the formula given as:

$$\delta = (z - z_0) - (d - d_0)m \quad (3)$$

where $z - z_0$ is the displacement of the cantilever. The ceramic nanofibers in this work were regarded as solid, so I could be obtained by the following formula:

$$I = \pi D^4/64 \quad (4)$$

where D is the diameter of the beam.

The elastic modulus of Al_2O_3-SiO_2-B_2O_3 nanofibers obtained at 800, 1000, 1200 and 1400 °C are shown in Fig. 8. The diameters of the four nanofibers acquired from the 2D AFM images by measuring the height of the deposited fibers were 413 nm, 425 nm, 439 nm and 420 nm, respectively. The elastic modulus of the fiber obtained at 800 °C was 9.47 ± 1.91 GPa, which revealed that the flexibility was quite good. XRD showed that no crystal phase generated at this temperature. For nanofibers in amorphous phase, atoms were less constrained and the bond energy was not too strong. Therefore, the nanofibers were easy to deform under stress from the radial direction, and consequently led to a low elastic modulus. The sample prepared at 1000 °C displayed an elastic modulus of 13.00 ± 2.28 GPa. The modulus increased by about 34% as compared with that of the sample prepared at 800 °C. This was because that the reaction between Al_2O_3 and B_2O_3 lowered the content of amorphous phase and the formative $Al_4B_2O_9$ crystal grains had the effect to impede deformation. With respect to the nanofiber prepared at 1200 °C, the elastic modulus increased to 18.19 ± 1.26 GPa. Tao et al. [44] studied the elastic modulus of $Al_4B_2O_9$ and $Al_{18}B_4O_{33}$ nanowires and drew the conclusion that $Al_{18}B_4O_{33}$ nanowires have higher elastic modulus. Thus, one reason for the increase in elastic modulus would be the transformation of phase composition from $Al_4B_2O_9$ to $Al_{18}B_4O_{33}$. Besides, the reduction of amorphous SiO_2, the formation of mullite and the growth of crystal grains also contributed to higher modulus. After calcining at 1400 °C, the nanofibers exhibited an elastic modulus of 27.30 ± 2.61 GPa. As discussed above, to fibers obtained at this temperature, very few $Al_{18}B_4O_{33}$ and amorphous silica existed, mullite had been the dominant component and the grains was the largest. Therefore, the modulus value was the highest, which indicated that the flexibility of the nanofibers was the worst.

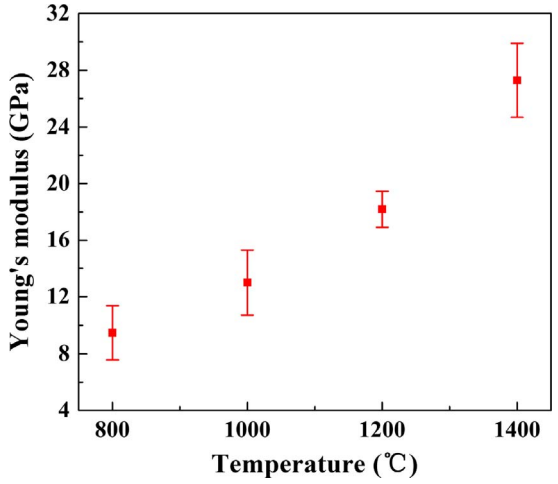

Fig. 8. Elastic modulus of Al_2O_3-SiO_2-B_2O_3 nanofibers obtained at elevated temperatures.

It was evident that the modulus values of the Al_2O_3-SiO_2-B_2O_3 nanofibers were much lower than that of the Nextel™ 312 fibers. Many factors led to such difference. A significant one was that the higher surface-to-volume ratio of the nanofibers. Atoms on fiber surface were less constrained than those in the inner [45], therefore, electrospun ceramic nanofibers with higher surface-to-volume ratio were easier to deform than the commercial fibers. Consequently, lower elastic modulus was achieved. Beyond that, tiny voids and cracks would generate in electrospun ceramic fibers due to the use of PVP [46], whose existence promoted the fiber deformation, thereby leading to a lower modulus.

Al_2O_3-SiO_2-B_2O_3 nanofiber mats obtained at 1000 °C, 1200 °C and 1400 °C were bended and folded to test their flexibility. The optical photographs and SEM images of the bended and folded fiber mats are shown in Fig. 9. As seen in Fig. 9(a), details of optical photograph of the fiber mat exhibited no fractures when it was bended to ~ 0.5 mm radius and the bended fiber mat kept the intact form after releasing. The SEM image in Fig. 9(b) showed that the nanofibers retained continuous structure when they were folded to a very small radius. While for the fiber mat prepared at 1200 °C as displayed in Fig. 9(c), the fiber mat could not be bended to the arc structure and a folding line was observed. The released mat could not retain the intact form since visible and irreparable cracks generated. The mat would eventually break into two pieces when bended it for two or three times. SEM image of the folded region (Fig. 9(d)) revealed that though some nanofibers were continuous, a large fraction of broken fibers emerged. When the calcination temperature increased to 1400 °C, the fiber mat fractured into pieces while bending it (Fig. 9(e)), revealing that the nanofibers could not deform. This could be testified by the SEM image of the folded mat as displayed in Fig. 9(f) since all nanofibers broke into two parts at around the folded region. These results were in consistent with the results of the elastic modulus. Considering the outstanding flexibility of the composite nanofiber mat prepared at 1000 °C, it would be easy to convert the fiber product into required shapes or forms. This is significant for expanding its practical applications, e.g. ceramic nanofiber based nanocomposites, high-performance auto exhaust catalyst supports, filtration materials for high-temperature filters, and insulation membrane for subtle objects to keep them from being destroyed during their service lifetime under high temperatures.

4. Conclusions

For Al_2O_3-SiO_2-B_2O_3 composite nanofibers prepared at elevated temperatures, $Al_4B_2O_9$ phase, instead of γ–Al_2O_3 or mullite, formed first at 900 °C due to the reaction between Al_2O_3 and B_2O_3. When calcination temperature reached up to 1100 °C, $Al_4B_2O_9$ transformed to $Al_{18}B_4O_{33}$ and mullite formed as well. The crystal grains grew bigger at higher preparation temperatures, which made the surface of the continuous nanofibers turn from smooth to rough. To ascertain the dominant phase between $Al_{18}B_4O_{33}$ and mullite by XRD, FT-IR or TEM and to distinguish the $Al_{18}B_4O_{33}$ grains and mullite grains by HRTEM were difficult since the two phases had similar crystal structure and lattice parameters. The elastic modulus increased constantly with the elevated calcination temperatures. The nanofibers obtained at 1000 °C displayed excellent flexibility owing to the small $Al_4B_2O_9$ grains and the large content of amorphous SiO_2.

Acknowledgement

The authors gratefully acknowledge the financial support from the “Chang Jiang Scholars Program” of the Ministry of Education of China

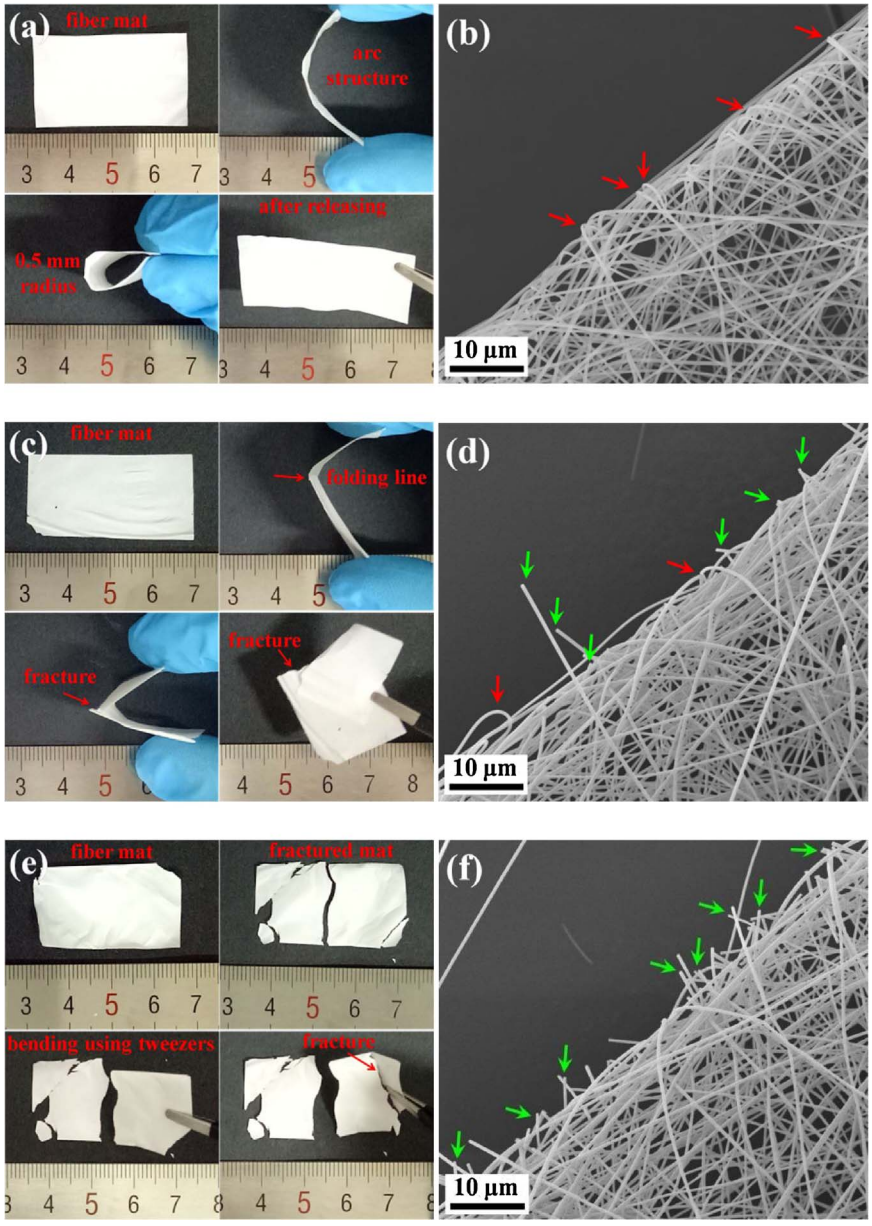

Fig. 9. Optical photographs and SEM images of the bended and folded Al_2O_3-SiO_2-B_2O_3 nanofiber mat obtained at (a) (b) 1000 °C, (c) (d) 1200 °C and (e) (f) 1400 °C. Red and green arrows in (b) (d) and (f) show the continuous and fractured nanofibers, respectively. (For interpretation of the references to colour in this figure legend, the reader is referred to the web version of this article.)

(Grant no. T2011119).

References

[1] A.R. Bunsell, M.H. Berger, Fine diameter ceramic fibres, J. Eur. Ceram. Soc. 20 (2000) 2249–2260.
[2] C.J. Armani, M.B. Ruggles-Wrenn, R.S. Hay, G.E. Fair, Creep and microstructure of Nextel™ 720 fiber at elevated temperature in air and in steam, Acta Mater. 61 (2013) 6114–6124.
[3] D. Schawaller, B. Clauß, M.R. Buchmeiser, Ceramic filament fibers — a review, Macromol. Mater. Eng. 297 (2012) 502–522.
[4] T.L. Tompkins, Ceramic oxide fibers: building blocks for new applications, Ceram. Ind. 144 (1995) 45–48.
[5] E.A. Richards, C.J. Goodbrake, H.G. Sowman, Reactions and microstructure development in mullite fibers, J. Am. Ceram. Soc. 74 (1991) 2404–2409.
[6] D.D. Johnson, Nextel 312 ceramic fiber from 3 M, J. Ind. Text. 10 (1982) 282–296.
[7] Z. Zhao, X. Shen, H. Yao, J. Wang, J. Chen, Z. Li, Alumina nanofibers obtained via electrospinning of pseudo-boehmite sol/PVP solution, J. Sol-Gel Sci. Technol. 70 (2014) 72–80.
[8] A. Mahapatra, B.G. Mishra, G. Hota, Synthesis of ultra-fine α-Al_2O_3 fibers via electrospinning method, Ceram. Int. 37 (2011) 2329–2333.
[9] P. Zhang, X. Jiao, D. Chen, Fabrication of electrospun Al_2O_3 fibers with CaO-SiO_2 additive, Mater. Lett. 91 (2013) 23–26.
[10] M. Allahverdi, R.A.L. Drew, M. Engineering, Melt-extracted oxide ceramic fibres-the fundamentals, J. Mater. Sci. 31 (1996) 1035–1042.
[11] S. Bernard, M. Weinmann, P. Gerstel, P. Miele, F. Aldinger, Boron-modified polysilazane as a novel single-source precursor for SiBCN ceramic fibers: synthesis, melt-spinning, curing and ceramic conversion, J. Mater. Chem. 15 (2) (2005) 289–299.
[12] Z. Xiao, B.S. Mitchell, The production of mullite fibers via inviscid melt-spinning (IMS), Mater. Lett. (1998) 359–365.
[13] W. Li, J. Wang, Z. Xie, H. Wang, Y. Tang, Preparation of hollow Si-B-N ceramic fibers by partial curing and pyrolysis of polyborosilazane fibers, Mater. Lett. 78 (2012) 1–3.
[14] J. Chandradass, M. Balasubramanian, Sol-gel processing of alumina fibres, J. Mater. Process. Technol. 173 (2006) 275–280.
[15] K. Song, K. Woo, Y. Kang, Preparation of alumina fibers from aluminum salts by the sol-gel method, Korean J. Chem. Eng. 16 (1999) 75–81.
[16] K. Okada, S. Yasohama, S. Hayashi, A. Yasumori, Sol-gel synthesis of mullite long fibres from water solvent systems, J. Eur. Ceram. Soc. 18 (1998) 1879–1884.
[17] H. Dai, J. Gong, H. Kim, D. Lee, A novel method for preparing ultra-fine alumina-borate oxide fibres via an electrospinning technique, Nanotechnology 13 (2002) 674.
[18] M. Krissanasaeranee, T. Vongsetskul, R. Rangkupan, P. Supaphol, S. Wongkasemjit, Preparation of ultra-fine silica fibers using electrospun poly(vinyl alcohol)/silatrane Composite Fibers as Precursor, J. Am. Ceram. Soc. 91 (2008) 2830–2835.
[19] J.-H. Kim, S.-J. Yoo, D.-H. Kwak, H.-J. Jung, T.-Y. Kim, K.-H. Park, J.-W. Lee, Characterization and application of electrospun alumina nanofibers, Nanoscale Res. Lett. 9 (2014) 44.
[20] R.W. Tuttle, A. Chowdury, E.T. Bender, R.D. Ramsier, J.L. Rapp, M.P. Espe, Electrospun ceramic fibers: composition, structure and the fate of precursors, Appl. Surf. Sci. 254 (2008) 4925–4929.

[21] J. Wu, H. Lin, J.B. Li, X.B. Zhan, J.F. Li, Fabrication and characterization of electrospun mullite nanofibers, Mater. Lett. 63 (2009) 2309–2312.
[22] M. Mohammad Ali Zadeh, M. Keyanpour-Rad, T. Ebadzadeh, Synthesis of mullite nanofibres by electrospinning of solutions containing different proportions of polyvinyl butyral, Ceram. Int. 39 (2013) 9079–9084.
[23] M. Mohammad Ali Zadeh, M. Keyanpour-Rad, T. Ebadzadeh, Effect of viscosity of polyvinyl alcohol solution on morphology of the electrospun mullite nanofibres, Ceram. Int. 40 (2014) 5461–5466.
[24] Z. Chen, Z. Zhang, C.C. Tsai, K. Kornev, I. Luzinov, M. Fang, F. Peng, Electrospun mullite fibers from the sol–gel precursor, J. Sol-Gel Sci. Technol. 74 (2015) 208–219.
[25] C. Peng, P. Liu, J. Hu, T. Hua, Y. Shen, B. Zhao, G. Tang, Preparation of uniaxially aligned mullite ceramic fibers by electrospinning, Colloids Surf. A Physicochem. Eng. Aspects 457 (2014) 1–7.
[26] S. Tanriverdi, B. Mavis, G. Gündüz, Ü. Çolak, Electrospinning and characterization of alumina borosilicate ceramic nanofibres, Mater. Sci. 25 (2007) 957–968.
[27] H.G. Sowman, Alumina–boria–silica ceramic fibers from the sol?gel process, in: L.C. Klein (Ed.), Sol–Gel Technoloy for Thin Films, Fibers, Performs, Electronics, and Specialty Shapes, Noyes, Park Ridge, NJ, 1988, pp. 162–182.
[28] S. Peng, H. Jinwen, W. Wenwei, W. Xuehang, Preparation of aluminum borate whiskers by the molten salt synthesis method, Ceram. Int. 39 (2013) 7263–7267.
[29] E. Elssfah, C. Tang, From $Al_4B_2O_9$ nanowires to $Al_{18}B_4O_{33}$: Eu nanowires, J. Phys. Chem. C. 111 (2007) 8176–8179.
[30] K.J. Griesser, A. Beran, D. Voll, H. Schneider, Boron incorporation into mullite, Mineral. Petrol. 92 (2008) 309–320.
[31] G. Zhang, Z. Fu, Y. Wang, H. Wang, W. Wang, J. Zhang, S.W. Lee, K. Niihara, Boron-doped mullite derived from single-phase gels, J. Eur. Ceram. Soc. 30 (2010) 2435–2441.
[32] L.S. Cividanes, T.M.B. Campos, L.A. Rodrigues, D.D. Brunelli, G.P. Thim, Review of mullite synthesis routes by sol-gel method, J. Sol-Gel Sci. Technol. 55 (2010) 111–125.
[33] A. Delmastro, G. Gozzelino, D. Mazza, M. Vallino, G. Busca, V. Lorenzelli, U. Genova, P.I. Kennedy, Characterization of microporous amorphous alumina-boria, J. Chem. Soc. Faraday Trans. 88 (1992) 2065–2070.
[34] M. Fisch, T. Armbruster, D. Rentsch, E. Libowitzky, T. Pettke, Crystal-chemistry of mullite-type aluminoborates $Al_{18}B_4O_{33}$ and Al_5BO_9: A stoichiometry puzzle, J. Solid State Chem. 184 (2011) 70–80.
[35] D. Voll, P. Angerer, A. Beran, H. Schneider, A new assignment of IR vibrational modes in mullite, Vib. Spectrosc. 30 (2002) 237–243.
[36] Y. Zhang, Y. Ding, J. Gao, J. Yang, Mullite fibres prepared by sol-gel method using polyvinyl butyral, J. Eur. Ceram. Soc. 29 (2009) 1101–1107.
[37] J. Leivo, M. Lindén, J.M. Rosenholm, M. Ritola, C.V. Teixeira, E. Levänen, T.A. Mäntylä, Evolution of aluminosilicate structure and mullite crystallization from homogeneous nanoparticulate sol-gel precursor with organic additives, J. Eur. Ceram. Soc. 28 (2008) 1749–1762.
[38] H. Lührs, R.X. Fischer, H. Schneider, Boron mullite: formation and basic characterization, Mater. Res. Bull. 47 (2012) 4031–4042.
[39] Y. Dai, W. Liu, E. Formo, Y. Sun, Y. Xia, Ceramic nanofibers fabricated by electrospinning and their applications in catalysis environmental science, and energy technology, Polym. Adv. Technol. 22 (2011) 326–338.
[40] S.H. Hong, W. Cermignani, G.L. Messing, Anisotropic grain growth in seeded and B_2O_3-doped diphasic mullite gels, J. Eur. Ceram. Soc. 16 (1996) 133–141.
[41] Y. Ding, P. Zhang, Y. Jiang, F. Xu, J. Yin, Y. Zuo, Mechanical properties of nylon-6/SiO_2 nanofibers prepared by electrospinning, Mater. Lett. 63 (2009) 34–36.
[42] E.P.S. Tan, C.T. Lim, Effects of annealing on the structural and mechanical properties of electrospun polymeric nanofibres, Nanotechnology 17 (2006) 2649–2654.
[43] A. Arinstein, E. Zussman, Electrospun polymer nanofibers: mechanical and thermodynamic perspectives, J. Polym. Sci. Part B Polym. Phys. 49 (2011) 691–707.
[44] X. Tao, X. Wang, X. Li, Nanomechanical characterization of one-step combustion-synthesized $Al_4B_2O_9$ and $Al_{18}B_4O_{33}$ nanowires, Nano Lett. 7 (2007) 3172–3176.
[45] X. Li, X.W. Xiong, P.C. Eklund, X. Li, X. Wang, S. Carolina, Top-down structure and device fabrication using in situ nanomachining, Appl. Phys. Lett. 87 (2005) 233113.
[46] X. Song, W. Liu, J. Wang, S. Xu, B. Liu, J. Liu, Y. Ma, Microstructural differences between electrospun alumina borate nanofibers prepared by solutions with different PVP contents, Ceram. Int. 43 (2017) 9831–9837.